Comparison of Equilibrium and Dynamic Properties of Polymethylene Melts of n-$C_{44}H_{90}$ Chains from Simulations and Experiments

Grant D. Smith[†] and Do Y. Yoon[*]

IBM Research Division, Almaden Research Center, 650 Harry Road, San Jose, California 95120-6099

Wei Zhu and M. D. Ediger

Department of Chemistry, University of Wisconsin—Madison, Madison, Wisconsin 53706

Received January 13, 1994; Revised Manuscript Received May 19, 1994[⊗]

ABSTRACT: Results of molecular dynamics simulations of n-$C_{44}H_{90}$ melts, based on an explicit atom model that reproduced experimental equilibrium and dynamic properties of n-$C_{13}H_{28}$ melts, were found to reproduce experimentally observed P–V–T behavior and X-ray scattering profiles of the higher molecular weight system. Moreover, the simulated local chain dynamics yielded ^{13}C NMR spin–lattice relaxation times (T_1) and the nuclear Overhauser enhancement (NOE) in quite good agreement with experimental values measured for different carbon positions and temperatures. The C–H vector P_2 autocorrelation functions for the interior carbons from the simulations exhibited long-time tails that yielded NOE values less than 3.0. The experimental T_1 values for the internal carbons of n-$C_{44}H_{90}$ in the melt differed only by a factor of 2 from those found for a high molecular weight polyethylene chain in the melt, indicating that a reasonably good understanding of local polymer dynamics is possible from our simulations of n-$C_{44}H_{90}$. Correlation times of the torsional autocorrelation function and the C–H vector reorientation for interior carbons were found to correspond to the average conformational transition times. Moreover, preliminary examination of the conformational transitions shows strong correlation with the neighboring bonds, especially with the second and fourth neighbors.

Introduction

In this paper the equilibrium and dynamic properties of polymethylene melts from molecular dynamics (MD) simulations are investigated using an explicit atom (EA) force field, where hydrogen atoms are considered explicitly. Previously,[1] it was found that equilibrium and dynamic properties of n-tridecane ($C_{13}H_{28}$) melts predicted from MD simulations using the EA force field were in good agreement with experimental values from, for example, X-ray diffraction, self-diffusion, and ^{13}C NMR spin–lattice relaxation experiments. Here we investigate the equilibrium and local dynamic properties of a much longer polymethylene chain, n-$C_{44}H_{90}$ (C_{44}), in the melt. We also investigate local chain dynamics in C_{44} and polyethylene melts experimentally via ^{13}C NMR T_1 and NOE measurements and compare simulation results with experiment. The present study includes a brief discussion of the correlation of conformational transitions in the bulk melt. In a future paper,[2] the overall chain dynamics in C_{44} melts will be discussed and a detailed analysis of local motions will be presented.

Simulation Methodology

The constant temperature and volume algorithm employed in the MD simulations is described in the previous paper.[1] As before, bond lengths were constrained while all other degrees of freedom remained flexible. The explicit atom force field is given in the previous paper.[1] The system consisted of 45 C_{44} molecules with periodic boundary conditions. The volume of the system at each simulation temperature, specifically 400 and 450 K, was determined so as to yield experimental densities, resulting in a periodic box dimension of approximately 40 Å. Nonbonded interactions were truncated at 6 Å, which was found to be adequate for the n-tridecane system.[1] Suitable long-range corrections were included in calculations of the pressure. An integration time step of 1.0 fs was utilized. After an equilibration time of approximately 500 ps, a series of five 100 ps sampling runs was performed at 450 K and a series of ten 100 ps runs was performed at 400 K. Reported error bars and uncertainties are standard 68% confidence limit values.

NMR Experiments

^{13}C nuclear Overhauser enhancement (NOE) and proton-decoupled spin–lattice relaxation time (T_1) measurements were performed at a ^{13}C Larmor frequency of 90.6 MHz using a Bruker AM-360 spectrometer.[3] The n-$C_{44}H_{90}$ sample (Aldrich) was used as received. Peak assignments were based upon those of Lyerla et al.[4] Separate peaks were observed for α, β, γ, and δ carbons. A single peak was observed in the proton-decoupled spectrum for all other carbons. Measurements were also performed on a high molecular weight polyethylene (PE) sample (high-density PE from Scientific Polymer Products, molecular weight approximately 125 000). Only a single line was observed in the proton-decoupled spectrum. In all T_1 measurements, the magnetization decayed as a single exponential within experimental error. Measurements are reported for C_{44} and PE from their melting points (361 and 393 K, respectively) to 425 K. Temperatures are accurate to ±2 K. Errors in T_1 values are ±10% unless otherwise indicated. NOE values are accurate to ±0.2. Samples were degassed prior to sealing. The PE T_1 values reported here are in good agreement with an extrapolation of previous measurements at lower temperature.[5] Extrapolated PE NOE values are not in agreement with one set of previous measurements by Dechter et al.[5] We do not know the reason for this discrepancy.

Equilibrium Properties

Chain Conformations. The chain dimensions of C_{44} are represented by the mean-square radius of gyration ratio $\langle s^2 \rangle / nl^2$, where n is the number of bonds (43 for C_{44}), $\langle s^2 \rangle$ is the mean-square radius of gyration of the chains, and l is the bond length. At 400 K a value of 0.96 ± 0.07

[†] Mailing address: Thermosciences Institute, RTC 230-3, NASA Ames Research Center, Moffett Field, CA 94035.

[⊗] Abstract published in *Advance ACS Abstracts*, August 1, 1994.

0024-9297/94/2227-5563$04.50/0

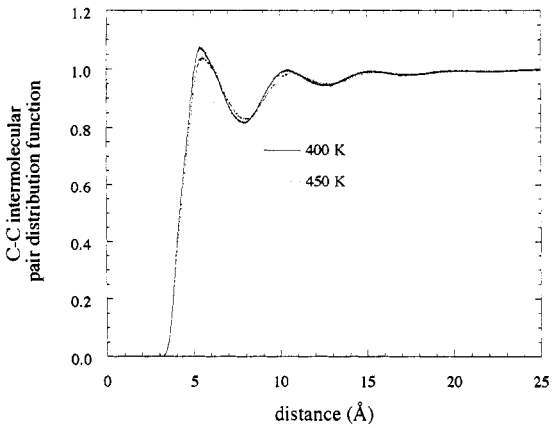

Figure 1. Carbon–carbon intermolecular pair distribution function for C_{44} melts.

was obtained, while at 450 K the simulations yielded a value of 0.94 ± 0.07. These values are in reasonable agreement with the predictions of the three-state rotational isomeric state model (RIS) of Flory,[6] which yields values of 0.86 and 0.82 at 400 and 450 K, respectively. As was found for *n*-tridecane,[1] the chain dimensions from the simulations are somewhat more extended than the RIS predictions. This is also reflected in the characteristic ratio for the chains, $\langle R^2\rangle/nl^2$, where $\langle R^2\rangle$ is the mean-square end-to-end distance. Simulations yield values of 7.4 and 7.0 at 400 and 450 K, respectively, compared to RIS values of 6.1 and 5.8. The uncertainty in the characteristic ratio values from the simulations is greater than that for the radius of gyration because of poorer statistics. The fraction of torsions in the trans state, $-60 \le \phi \le 60°$, was 0.61 at 400 K and 0.59 at 450 K, as compared with the RIS values of 0.60 and 0.58, respectively. The trans fraction for the C_{44} melt at 450 K is slightly greater than the value of 0.58 found for *n*-tridecane melt at the same temperature.[1]

***P–V–T* Behavior.** At experimental densities, the EA model employed yielded a pressure of −240 ± 27 atm at 450 K, with a similar value at 400 K, indicating that thermal expansion of C_{44} melts is reproduced reasonably well by the model. This pressure is similar to that yielded by the same force field in simulations of *n*-tridecane at experimental density (−175 ± 10 atm at 450 K). It is of interest to note that the united atom force field (where methylene and methyl groups are treated as single force centers) used in the previous study,[1] while yielding a reasonable pressure of −248 atm at 450 K for *n*-tridecane at experimental density, yielded a pressure of −650 atm at 450 K for C_{44} at experimental density. This discrepancy indicates that caution should be employed in using a single united atom force field for chains of different molecular weight.

Positional Order. The intermolecular pair distribution function for carbon atoms is shown for C_{44} at 400 and 450 K in Figure 1. Two well-defined maxima or peaks, corresponding to the nearest neighbor and next nearest neighbor interchain distances, are apparent at each temperature. The peaks are somewhat sharper at the lower temperature, reflecting an increase in positional order with decreasing temperature. The shift of peak position to shorter distances with decreasing temperature reflects the higher density of the low-temperature melt. Compared to *n*-tridecane at 450 K,[1] the 450 K C_{44} C–C pair distribution function shows peaks which are significantly sharper and shifted toward shorter distances, reflecting the higher density of the higher molecular weight system.

The characteristics of the intermolecular X-ray scattering peak for C_{44} melts determined from simulation at 450 K are compared with experimental values[7] for *n*-tridecane and PE at the same temperature in Table 1. It was found previously[1] that the characteristics of the intermolecular X-ray scattering peak for *n*-tridecane from simulations reproduced experimental values quite well. It is therefore apparent from Table 1 that positional order in C_{44} more closely resembles that in PE than that in the low molecular weight *n*-tridecane.

Table 1. Characteristics of the Intermolecular X-ray Scattering Peak in C_{44} Melts at 450 K

		exptl	
characteristic	calcd C_{44}	*n*-tridecane	PE
q_{max}[a,b]	1.29	1.26 (1.26)[c]	1.29
FWHM[b,d]	0.43	0.49 (0.51)	0.41

[a] $q = 4\pi \sin\theta/\lambda$, where 2θ is the scattering angle and λ is the wavelength of the scattered radiation. Units of q are Å^{-1}. [b] Data are from scattering intensity curves. Experimental data are from ref 6. [c] Values in parentheses are simulation results for *n*-tridecane from ref 1. [d] Full width of diffraction peak at half-maximum, in q.

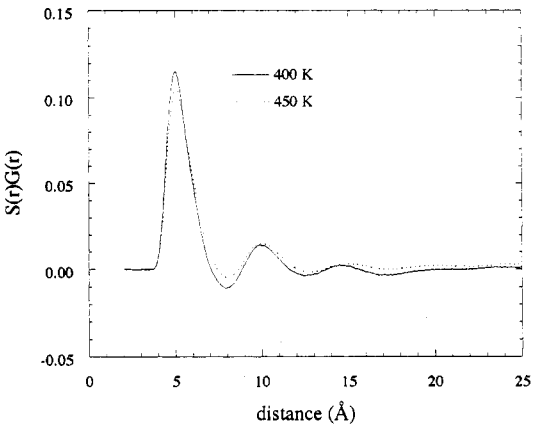

Figure 2. Weighted intermolecular orientational correlation function for two-bond segments in C_{44} melts.

Orientational Order. Orientational order in C_{44} melts was investigated by calculating the intermolecular orientational correlation function for two-bond segments, given by

$$S(r) = \frac{1}{2}[3\langle\cos^2\theta(r)\rangle - 1] \quad (1)$$

where θ is the angle formed by the vectors (one for each two-bond segment) bisecting the bonds forming the segment and r is the distance between the centers of the bisecting vectors. The angular brackets indicate an ensemble average over all such intermolecular segment pairs. The intermolecular orientational correlation functions, multiplied by the two-bond segment pair distribution function $G(r)$, are displayed in Figure 2 for C_{44} melts at 400 and 450 K. As in the carbon–carbon intermolecular pair distribution function (Figure 1), the intermolecular orientational correlation function shows two distinct maxima. Orientational order can be seen to increase with decreasing temperature. Compared to *n*-tridecane at 450 K,[1] the C_{44} melt at the same temperature shows significantly greater orientational correlation, with the peaks being much sharper and higher than was found for the low molecular weight material. At 400 K the C_{44} melt shows a definite peak even at the third nearest neighbor distance, reflecting the presence of fairly significant orientational correlation in the system.

Local Chain Dynamics

Torsional Dynamics. The dynamics of conformational transitions were investigated by monitoring the rates of conformational transitions and the rates of rotational

Table 2. Rates of Conformational Transitions and Barrier Crossings

temp (K)	(per 100 ps) rates: transitions	(per 100 ps) rates: barrier crossings	ratio	transition time (ps)
400	6.2 ± 0.1	25.3 ± 0.8	0.24	16.2
450	9.7 ± 0.2	35.4 ± 0.6	0.27	10.3

barrier crossings. A conformational transition is assumed to have occurred when a torsional angle moves from one conformational state ($-60 \le t < 60°$, $60 \le g^+ \le 180°$, $-180 \le g^- < -60°$) to the local conformational energy minimum associated with another conformational state ($t = 0°$, $g^\pm = \pm 114°$). A rotational barrier crossing occurs every time the torsion passes beyond the local conformational energy barrier (maximum) separating two states. Each C–C–C–C torsion was checked every time step for the occurrence of conformational transitions and barrier crossings. The transition and barrier crossing rates were calculated by dividing the total number of transitions and barrier crossings, respectively, for the entire system during a simulation run by the product of the total number of C–C–C–C torsions and the time of the simulation. As was found in n-tridecane,[1] the rates of barrier crossings are always greater than the transition rates because a fair number of torsions will cross a barrier without reaching the energy minimum of the "new" state. The conformational transition rates and rates of barrier crossings are shown in Table 2 for C_{44} at 400 and 450 K. The table also shows average times for conformational transitions, given as the reciprocal of the transition rates.

As was found for n-tridecane,[1] the fraction of barrier crossings leading to a complete transition increases with increasing temperature. At 450 K the fraction of barrier crossings leading to complete transitions is noticeably lower in C_{44} (0.27) than was found in n-tridecane (0.34[1]) at the same temperature. The activation energy, determined from the temperature dependence of the transition rates, assuming Arrhenius behavior, is 3.2 kcal/mol for C_{44}, essentially identical to the 3.1 kcal/mol[1] obtained for n-tridecane. The rate of barrier crossings at 450 K in C_{44} is less than 10% lower than in n-tridecane at the same temperature, while the transition rate is about 25% lower for the longer chains. For both C_{44} and n-tridecane, the activation energy for conformational transitions is near that for a single, isolated transition in butane of 3.0 kcal/mol (for the force field employed here), implying that matrix effects do not contribute significantly to the mean activation energy in the temperature range investigated. However, the relative decrease in the fraction of barrier crossings that lead to complete transitions for the longer chains, and the corresponding decrease in the transition rate, may reflect influences of the surrounding matrix on the ability of the chain geometry to adjust to transitions by restricting the ability of neighboring torsions to distort. The greater transition rate in the low molecular weight material would therefore be due primarily to the higher fraction of torsions near the relatively unrestricted ends of the chain and not to density effects.

As in n-tridecane,[1] torsional dynamics were investigated by monitoring the torsional angle autocorrelation function

$$P(t) = \frac{\langle \cos\phi(t) \cos\phi(0)\rangle - \langle \cos\phi(0)\rangle^2}{\langle \cos\phi(0) \cos\phi(0)\rangle - \langle \cos\phi(0)\rangle^2} \qquad (2)$$

where the angular brackets indicate an ensemble average over all torsions and $\phi(t)$ is the torsional angle at time t. The torsional angle autocorrelation functions at 400 and 450 K are displayed in Figure 3. The autocorrelation functions were fit with the KWW equation

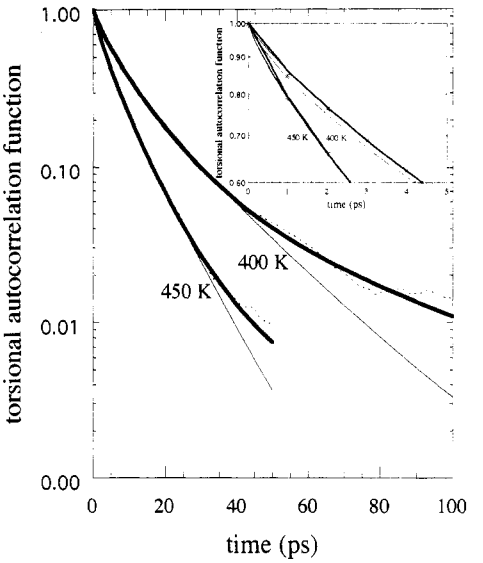

Figure 3. Torsional autocorrelation function in C_{44} melts. The dashed lines are the autocorrelation functions from simulations. The thin solid lines are a fit of the KWW equation (eq 3) to the simulation data, while the thick solid lines are a fit of eq 5 to the simulation data. The insert shows the short-time behavior of the torsional autocorrelation function. The symbols indicate the simulation data.

$$P_{KWW}(t) = \exp[-(t/\tau)^\beta] \qquad (3)$$

The resulting fits are also shown in Figure 3. Average KWW parameters are shown in Table 3, along with correlation times calculated using

$$\tau^c_{KWW} = \int_0^\infty P_{KWW}(t)\, dt \qquad (4)$$

Examination of Figure 3 indicates that while the KWW equation fits the torsional autocorrelation reasonably well, it does decay more rapidly at longer times. This is especially apparent at 400 K. We refer to this persistence of correlation to very long times as the long-time tail behavior. Such behavior was not seen in the torsional autocorrelation function for n-tridecane,[1] even at 312 K. We have attempted to describe the long-time tail with a single exponential with relaxation time τ_{tail}, or

$$P_{total}(t) = A \exp[-(t/\tau)^\beta] + (1 - A) \exp(-t/\tau_{tail}) \qquad (5)$$

with

$$\tau^c_{total} = \int_0^\infty P_{total}(t)\, dt \qquad (6)$$

The resulting fit, which is much improved, is illustrated in Figure 3. Some discrepancy can be seen for very short times (<2 ps; see insert in Figure 3). Parameter values are shown in Table 3. An indication of the effect of the long-time tail is to express eq 6 as

$$\tau^c_{total} = A\int_0^\infty \exp[-(t/\tau)^\beta]\, dt + (1 - A)\int_0^\infty \exp(-t/\tau_{tail})\, dt$$

$$= A\tau^c_{KWW,tail} + (1 - A)\tau^c_{tail} \qquad (7)$$

where the τ and β parameters are from the fits with tails. The correlation times $\tau^c_{KWW,tail}$ and τ^c_{tail} are given in Table 3. The long-time tail contribution, $(1 - A)\tau^c_{tail}$, is about 10% of the total torsional correlation time at 450 K and almost 30% at 400 K.

We do not wish to imply that the functional form of eq 5 has any particular physical significance. Many other functional forms have been suggested based on specific

Table 3. Torsional Autocorrelation Function Parameters

	KWW only			KWW + tail						
temp	τ (ps)	β	τ^c_{KWW} (ps)	τ (ps)	β	τ_{tail} (ps)	A	$\tau^c_{KWW,tail}$ (ps)	τ^c_{tail} (ps)	τ^c_{total} (ps)
400	10.1 ± 0.3	0.76 ± 0.05	11.9 ± 1.0	9.0	0.84	53	0.931	9.8	53	12.8
450	5.9 ± 0.2	0.80 ± 0.03	6.6 ● 0.3	5.7	0.83	41	0.982	6.3	41	6.9

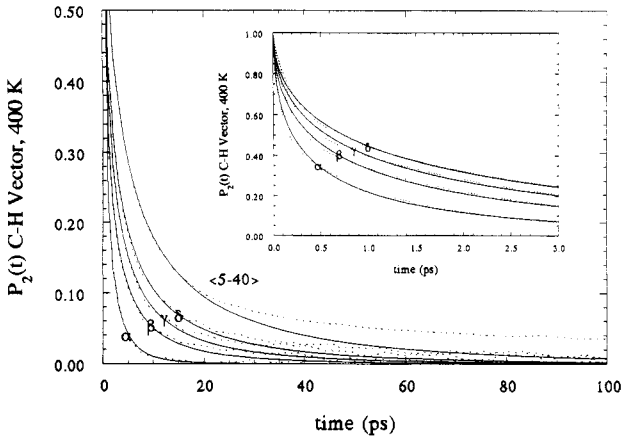

Figure 4. C–H vector P_2 autocorrelation function for selected carbons in C_{44} melts at 400 K. ⟨5–40⟩ is an average over the interior carbons. The dashed lines are the simulation data. The solid lines are a fit of the KWW equation (eq 3) to the short-time (≤20 ps) data. The insert illustrates the very short time (<5 ps) region.

models for local chain dynamics (e.g., see Viovy, Monnerie, and Brochon[8] and the references contained therein). Some of these may also fit our simulation results. We use eq 5 primarily as a convenient means of reproducing the simulation results. However, it may be that the two terms in eq 5 originate from different physical processes. Assuming Arrhenius behavior, τ^c_{total} has an activation energy of 4.4 kcal/mol. This value is significantly greater than the 3.2 kcal/mol obtained based upon the torsional transition rates (see above). In contrast, the torsional correlation times determined excluding the long-time tail, the $\tau^c_{KWW,tail}$ values in Table 3, yield an activation energy of 3.2 kcal/mol. In addition, these correlation times agree with the torsional transition times in Table 2. Thus the first term in eq 5 apparently reflects the torsional transition rate. The nature of the long-time tail will be discussed below and in detail in an upcoming paper.[2]

Simulation Results of C–H Vector Reorientation. Local dynamics can also be probed by monitoring the rate of reorientatin of C–H vectors. The C–H vector autocorrelation functions are given by

$$P_1^{CH}(i,t) = \langle \mathbf{CH}(i,t)\cdot\mathbf{CH}(i,0)\rangle \quad (8)$$

$$P_2^{CH}(i,t) = \frac{1}{2}(3\langle[\mathbf{CH}(i,t)\cdot\mathbf{CH}(i,0)]^2\rangle - 1) \quad (9)$$

where $\mathbf{CH}(i,t)$ is a unit vector lying along the vector direction from carbon atom i to an attached hydrogen atom at time t. The index i indicates the position of the carbon atom along the chain backbone.

The P_2^{CH} autocorrelation function is plotted in Figure 4 at 400 K for selected carbon atoms. The solid lines are fits of the KWW equation (eq 3) to short-time data (≤20 ps). Parameters and the resulting correlation times (eq 4) are shown in Table 4. Parameters and correlation times for the P_1 autocorrelation function are also shown. It can be seen in Figure 4 that the closer a carbon atom is to the chain center, the greater the discrepancy between the KWW fit and the autocorrelation function for longer times, i.e., the more significant the long-time tail. This effect

Table 4. Parameters and Correlation Times for the Short-Time Behavior of the C–H Vector Autocorrelation P_1 and P_2 Functions of C_{44} Melts

carbon	τ_1	β_1	$\tau^c_{1,KWW}$	τ_2	β_2	$\tau^c_{2,KWW}$
			400 K			
α	1.49[a]	0.56[b]	2.47[c]	0.48[c]	0.47[b]	1.06[a]
β	2.51[a]	0.68[b]	3.42[a]	0.86[a]	0.45[b]	2.12[a]
γ	3.42[c]	0.67[b]	4.49[c]	1.19[a]	0.44[b]	3.09[c]
δ	4.34[c]	0.70[b]	5.47[c]	1.59[a]	0.45[b]	4.01[c]
⟨5–40⟩	8.08[b]	0.69[a]	10.37[c]	3.03[b]	0.45[b]	7.51[c]
22	9.00[c]	0.65[a]	12.38[d]	3.33[c]	0.45[a]	8.40[c]
			450 K			
α	0.95[a]	0.59[b]	1.46[a]	0.31[a]	0.51[b]	0.60[a]
β	1.62[a]	0.70[b]	2.05[a]	0.57[a]	0.50[b]	1.15[a]
γ	2.06[a]	0.74[b]	2.46[a]	0.75[a]	0.48[b]	1.62[a]
δ	2.67[a]	0.75[b]	3.18[a]	0.97[a]	0.48[b]	2.15[c]
⟨5–40⟩	4.54[c]	0.71[b]	5.68[c]	1.57[a]	0.45[b]	3.99[a]
22	5.19[d]	0.65[a]	7.11[d]	1.81[c]	0.44[a]	4.65[c]

[a] Uncertainty of ±0.10 or less. [b] Uncertainty of ±0.02 or less. [c] Uncertainty of ±0.5 or less. [d] Uncertainty of ±1.0 or less.

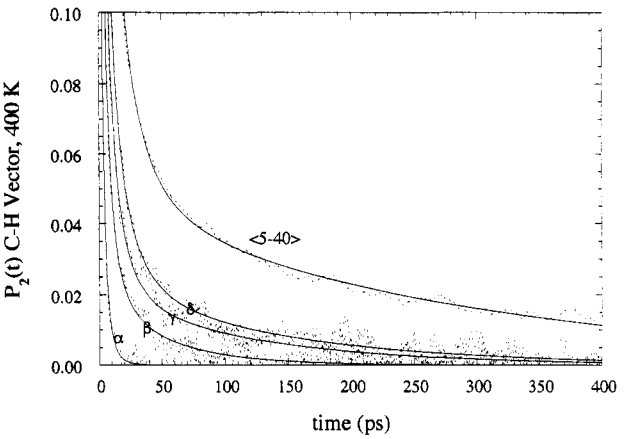

Figure 5. C–H vector P_2 autocorrelation function for selected carbons in C_{44} melts at 400 K. ⟨5–40⟩ is an average over the interior carbons. The dashed lines are the simulation data. The solid lines are a fit equation (eq 5) to the simulation data.

was not seen to any significant degree for the low molecular weight n-tridecane. As with the torsional autocorrelation function, we have fit the long-time tail to a single exponential (eq 5). The resulting fits at 400 K for the tail region of P_2 are shown in Figure 5. The corresponding parameters and correlation times (eq 6) at 400 and 450 K are given in Table 5.

Most of the decay in the amplitude of the autocorrelation function for the C–H vectors in C_{44} (>95% from the A parameter in Table 5) is the result of fast motions approximately described by the KWW equation. These motions are presumably very local. The effect of including the long-time tail on the τ^c_2 correlation times for the central carbon atoms is significant. We believe the long-time tail reflects the inability of C–H vectors for carbon atoms not near a chain end to decorrelate completely as a result of local torsional transitions alone. A complete decorrelation of these C–H vectors appears to involve motions with a time scale much longer than that of local torsional transitions, e.g., reorientation of longer segments of the molecule. This is consistent with the interpretation of NMR relaxation time measurements on polymers in solution and the bulk.[3,9,10] In the low molecular weight n-tridecane, the time scale for reorientation of the entire

Table 5. Parameters and Correlation Times for the C-H P_2 Vector Autocorrelation Function of C_{44} Melts, Including Long-Time Tail Effects[a]

carbon	τ_2 (ps)	β	τ_{tail} (ps)	A	$\tau^c_{2,total}$[a] (ps)
			400 K		
α	0.48	0.47	—[b]	—	1.1 ± 0.1
β	0.77	0.47	52	0.980	2.7
γ	1.07	0.46	122	0.980	4.9
δ	1.39	0.46	142	0.977	6.6
⟨5-40⟩	2.53	0.49	285	0.954	18.4
			450 K		
α	0.31	0.51	—	—	0.6 ± 0.1
β	0.57	0.50	—	—	1.2 ± 0.1
γ	0.66	0.51	57	0.982	2.3
δ	0.85	0.49	108	0.986	3.3
⟨5-40⟩	1.40	0.50	163	0.965	8.5

[a] Uncertainties for carbons with significant long-time tail effects were estimated from the scatter in the long-time tail contribution to the correlation times from different simulation runs (β, γ, and δ carbons) or from different carbons (for the central carbons). Estimated uncertainties are about 10% for the β, γ, and δ carbons and about 15–20% for the interior carbons. [b] Indicates negligible long-time tail.

molecule is not that much greater than that of the local torsional transitions. This is not the case, however, for the higher molecular weight C_{44}, where the time scale for reorientation of the molecule is much longer.[2]

NMR Measurements of C-H Vector Reorientation. ^{13}C T_1 and NOE measurements provide direct experimental information about the local dynamics of polymer chains. These observables are sensitive to the reorientation of bond vectors connecting a ^{13}C nucleus and its bonded protons. T_1 and NOE can be expressed in terms of the spectral density function $J(\omega)$:

$$\frac{1}{T_1} = Kn[J(\omega_H-\omega_C) + 3J(\omega_C) + 6J(\omega_H+\omega_C)] \quad (10)$$

$$\mathrm{NOE} = 1 + \frac{\gamma_H}{\gamma_C}\left[\frac{6J(\omega_H+\omega_C)}{J(\omega_H-\omega_C) + 3J(\omega_C) + 6J(\omega_H+\omega_C)}\right] \quad (11)$$

Here, γ_C and γ_H are the gyromagnetic ratios for carbon and hydrogen, ω_C and ω_H are their respective resonance frequencies, and n is the number of bonded protons. The constant K is taken to be 2.29×10^9 s^{-2}.[11] $J(\omega)$ is the Fourier transform of the orientation autocorrelation function for a C-H vector:

$$J(\omega) = \frac{1}{2}\int_{-\infty}^{+\infty} P_2^{CH}(t)e^{i\omega t}\,dt \quad (12)$$

Here $P_2^{CH}(t)$ is given by eq 9.

In the extreme narrowing regime, eqs 10 and 11 are simplified significantly:

$$\frac{1}{T_1} = 10nK\tau^c \quad (13)$$

$$\mathrm{NOE} = 1 + \frac{\gamma_H}{2\gamma_C} = 2.99 \quad (14)$$

The correlation time τ^c in eq 13 is the time integral of eq 9 from zero to infinity. Equation 13 is valid even for nonexponential correlation functions, provided extreme narrowing conditions apply.[3,4] Two possible systematic errors need to be considered when applying eqs 10–14. First, the constant K is known only to an accuracy of 5–10%. Second, dipolar relaxation due to nonbonded protons is not included in these equations. We estimate that this represents less than a 10% error for the case of C_{44} (see ref 10).

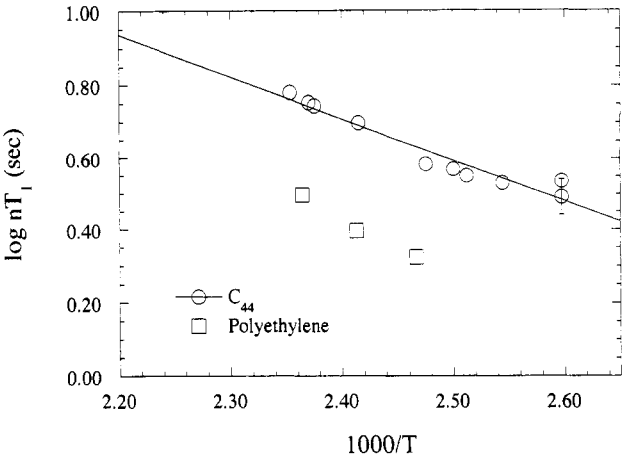

Figure 6. nT_1 values for C_{44} interior carbons and polyethylene melts as a function of temperature. Representative error bars for the experimental data are shown.

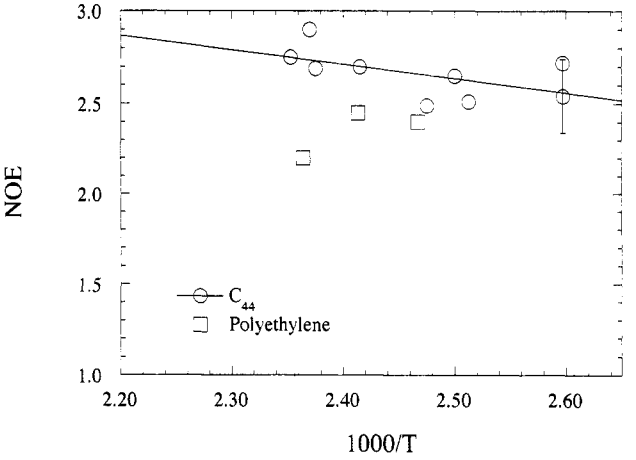

Figure 7. NOE values for C_{44} interior carbons and polyethylene melts as a function of temperature. Representative error bars for the experimental data are shown.

Table 6. Comparison of Simulation and Experimental Correlation Times of C_{44} Melts Assuming Extreme Narrowing Conditions

		simulation	exptl	
temp (K)	carbon	$\tau^c_{2,total}$[a] (ps)	τ^c (ps)	NOE
400	α	1.1 ± 0.1	1.2 ± 0.1	2.9 ± 0.2
	β	2.7	2.6 ± 0.3	3.0 ± 0.2
	γ	4.9	3.9 ± 0.4	2.9 ± 0.2
	δ	6.6	6.1 ± 0.9	3.0 ± 0.2
	⟨5-40⟩	18.4	11.1 ± 1.2[b]	2.64 ± 0.2
450	⟨5-40⟩	8.5	5.3 ± 0.7[b,c]	2.85 ± 0.2[c]

[a] Uncertainties estimated from the scatter in the long-time tail contribution to the correlation times (see footnote to Table 5) are about 10% for the β, γ, and δ carbons and about 15–20% for the interior carbons. [b] As extreme narrowing conditions do not appear to apply in these cases, the true correlation time will be somewhat greater than the value calculated assuming extreme narrowing conditions. [c] Extrapolated from lower temperature.

T_1 and NOE values for interior carbons in C_{44} (carbons 5–40) and PE are shown in Figures 6 and 7. For C_{44}, NOE is close to 3 in the temperature range of interest. Thus we initially compare the NMR measurements to the simulations using eq 13 to calculate τ^c. Table 6 shows this comparison with $\tau^c_{2,total}$ values from the simulation, which include the long-time tail effects. For the α through δ carbons at 400 K, NOE is equal to 3 within experimental error. Thus for these cases, the use of eq 13 is clearly justified. For these four carbons at the end of the chain, the agreement between experiment and simulation is excellent.

Table 7. Comparison of Simulated and Experimental ^{13}C T_1 and NOE Values in C_{44} Melts

		T_1 (s)		NOE	
temp (K)	carbon	simulation[a]	experiment	simulation[a]	experiment
400	α	13.2 ± 1.5	11.7 ± 1.2	2.99	2.9 ± 0.2
	β	8.0[b]	8.3 ± 0.8	2.98	3.0 ± 0.2
	γ	4.6[b]	5.6 ± 0.6	2.94	2.9 ± 0.2
	δ	3.5[b]	3.6 ± 0.6	2.92	3.0 ± 0.2
	⟨5-40⟩	1.5[b]	1.95 ± 0.2	2.68	2.64 ± 0.2
450	⟨5-40⟩	2.8[b]	4.1 ± 0.6[c]	2.87	2.85 ± 0.2[c]

[a] Determined using the autocorrelation representation in eq 5. [b] Uncertainties estimated from the scatter in the long-time tail contribution to the correlation times (see footnote to Table 5) yield uncertainties in T_1 from simulation of about 15–20%. [c] Extrapolated from lower temperatures.

The comparison between simulation and experiment shown in Table 6 is only approximately valid for the internal carbons since the observed NOE values are somewhat less than 3. Some of the differences between simulation and experiment for these carbons can be attributed to the use of eq 13 where it is not strictly justified. A more accurate comparison was performed using eq 12 and the full time dependence of the simulated correlation function (eq 5) to calculate $J(\omega)$. Equations 10 and 11 were then used to calculate T_1 and NOE at 90.6 MHz. These values are compared to the experimental results in Table 7.

Table 7 indicates excellent agreement between the measured and simulated NOE values. This clearly indicates that it is the long-time tails of the simulated correlation functions which cause the NOE values to be less than 3 in C_{44} melts. NOE values predicted from autocorrelation functions without the long tail (eq 4) are greater than 2.97 at both temperatures. For the α through δ carbons, excellent agreement between simulated and experimental values is seen. For the interior carbons, reasonable agreement between simulated and experimental T_1 values is also obtained. The roughly 30% smaller simulated T_1 values for the interior carbons indicate that the simulated local motions are somewhat slower than those observed in the experiment. Some of this difference between simulated and experimental T_1 values may be due to the uncertainty in the coupling constant K (see above). However, an error in K would also influence T_1 values for the four end carbons. Regardless of the value of K, one could restate the comparison of experiment with simulations as follows: The simulated chain dynamics show a greater dependence on carbon atom position than is indicated by experiment. It is also possible that a much longer simulation would reveal that eq 5 is not an adequate description of the correlation function shape. A more precise comparison between experiment and simulation would be possible with additional experimental observables (T_1, T_2, and NOE measurements at lower Larmor frequencies).

Our NMR measurements provide a rough indication of the extent to which the local dynamics of C_{44} represent those of high molecular weight PE. As shown in Figure 6, T_1 values for PE are about 2 times smaller than T_1 values for the interior carbons of C_{44}. As discussed above, two types of motions appear to contribute to the decay of the C–H vector autocorrelation function: torsional motions (transitions) and long-time motions whose time scale corresponds to reorientation of longer segments of the molecule. Hence, the difference in T_1 values for PE and the interior carbons of C_{44} are due to a slower rate of torsional transitions in PE, a more significant long-time component to the C–H vector reorientation, or a combination of these effects. Comparing the rate of torsional transitions in n-tridecane and C_{44}, the rate in C_{44} is only 25% slower at 450 K. As discussed above, positional order in C_{44} more closely resembles that in polyethylene than in n-tridecane. Additionally, the density difference between n-tridecane and C_{44} is greater than the difference between C_{44} and PE at 450 K. Finally, assuming a $1/N$ dependence of the influence of chain ends on the conformational dynamics, C_{44} again more closely resembles polyethylene than n-tridecane. Based on these considerations, it appears likely that the factor of 2 difference in T_1 values between PE and the central carbons of C_{44} is due mostly to differences in the long-time behavior of the C–H vector autocorrelation functions.

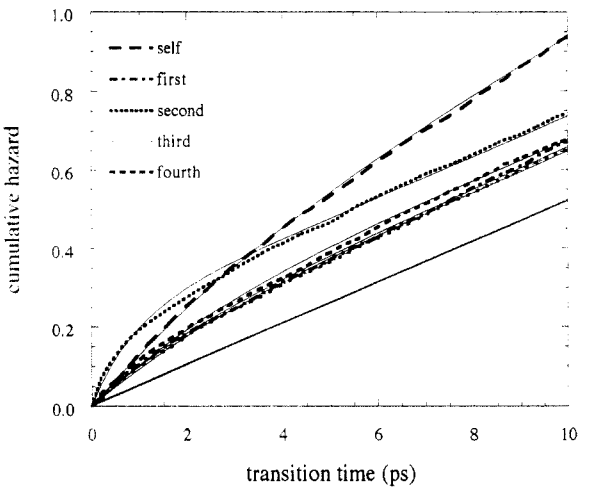

Figure 8. Cumulative Hazard plots for the central torsions of C_{44} chains at 400 K for self-transitions and first through fourth neighbor transitions. The solid lines are fits of eq 15 to the simulation data. The linear solid curve illustrates the behavior of a noncorrelated process with a rate of 0.05/ps.

Correlation of Conformational Transitions. The degree to which torsional transitions are correlated with transitions in neighboring torsions is of great importance in determining the mechanisms of local motions in chain molecules. Here we discuss briefly several salient features of correlation of torsional transitions in C_{44}. Correlation of transitions will be considered in detail in a future paper.[2]

In Brownian dynamics studies of "phantom chain" molecules, Helfand and co-workers[12,13] found significant second neighbor correlation, involving mostly gauche generation/annihilation ($ttt \rightleftarrows g^{\pm}tg^{\mp}$) and gauche migration ($g^{\pm}tt \rightleftarrows ttg^{\pm}$) mechanisms. A convenient method for examining the degree of correlation of torsional transitions in chain molecules is the cumulative Hazard plot.[12-14] Hazard plots were constructed from first passage times as described in ref 14. A first passage time corresponds to the time, after a reference torsion completes a transition, that the torsion (self) or a neighbor (first through fourth neighbors) completes a transition. Self and neighbor first passage times, up to the fourth neighbor, were determined for the central 9 bonds of each chain in an attempt to reduce the influence of the chain ends. The resulting Hazard plot at 400 K for C_{44} for self and first through fourth neighbors is shown in Figure 8. The Hazard data for the first through fourth neighbors were normalized by dividing by 2 to account for the fact that + and − neighbors were not separated in accumulating the first passage times. The solid lines correspond to a least-squares fit of the function[13]

$$H_i(t) = \lambda_i t + \nu_i[1 - \exp(-t/\sigma_i)] \qquad (15)$$

to the Hazard plot data. The fits are quite reasonable. The index i indicates self ($i = 0$) or neighbor ($i = 1$–4)

Table 8. Hazard Function Parameters for C_{44} Melts at 400 K

neighbor	index	λ_i (ps^{-1})	ν_i	σ_i (ps)	c_i
self	0	0.066	0.31	4.2	0.27 (0.27)
first	1	0.054	0.12	2.0	0.11
second	2	0.052	0.22	0.9	0.20 (0.12)
third	3	0.051	0.14	2.6	0.13
fourth	4	0.048	0.20	3.1	0.18

cumulative Hazards. The first term on the right corresponds to the cumulative Hazard for a simple Poisson process. Such a process is illustrated in Figure 8 for $\lambda = 0.05$ ps^{-1}. The second term quantifies the self ($i = 0$) or neighbor ($i = 1$–4) correlation, i.e., the degree to which transitions occur at a rate greater than the expected "background" Poisson rate λ_i. This term results in steeper initial slopes of the Hazard plots ($>\lambda_i$), as can be seen in Figure 8. The parameter σ_i describes the spread in time of the correlated transitions. A small value of σ_i indicates that the transitions are correlated over a short time and that the corresponding Hazard plot more rapidly approaches its limiting slope. The resulting parameters are shown in Table 8. Also shown for $i = 0$–4 is

$$c_i = 1 - \exp(-\nu_i) \tag{16}$$

which is a measure of the fraction of transitions which are correlated.[13] Shown in parentheses are results from Brownian dynamics simulations of phantom chains[13] at 400 K.

As was found in the Brownian dynamics simulations of phantom chains,[12,13] the C_{44} melt chains indicate a significant degree of self-correlation in torsional transitions, revealed by the large value of c_0. (It should be remembered that c_i reflects only those transitions which occur in response to the "triggering" transition of the reference torsion and do not count the triggering torsion itself.) Table 8 reveals that σ_0 is about 4 ps. This indicates that many of the self-correlated transitions are not simply immediate self-reversals (see discussion of σ_2 below), although many of these latter transitions do occur.[2] As was also seen previously,[12,13] we see significant second neighbor correlation. The relatively short σ_2 (0.9 ps) indicates that many of the correlated second neighbor transitions occur immediately after completion of the triggering transition, consistent with the gauche generation and migration mechanisms proposed by Helfand and coworkers.[12,13] However, even given the large uncertainty in c_i values of about ±0.05, it appears that the degree of second neighbor correlation is somewhat greater in our bulk melt simulation than was seen in the Brownian dynamics phantom chain simulations. Finally, first, third, and particularly fourth neighbor correlation is evident in Table 8. Comparison of σ_i values indicates that these correlations are of somewhat longer time than the second neighbor correlation but are of short time compared to the average transition time. Further discussion of correlation of conformational transitions, including comparison with results of previous studies, will be considered in a future paper.[2]

Conclusions

For X-ray scattering profiles and P–V–T behavior of C_{44} melts, good agreement was found between experiment and molecular dynamics simulations using an explicit atom model. The predicted P–V–T behavior of C_{44} melts using a united atom model, which successfully reproduced the equilibrium properties of n-tridecane, did not agree well with experimental values. Our simulation results show significant intermolecular orientational correlation that extends to third neighbor segments in C_{44} melts. Good agreement between experiments and simulations was also seen for local chain dynamics in C_{44} melts, as reflected in the reorientation of C–H vectors; predicted ^{13}C NMR spin–lattice relaxation times T_1, nuclear Overhauser enhancement NOE, and corresponding P_2 correlation times for C–H vectors as a function of carbon position and temperature were found to agree quite well with experimental values. Simulated C–H vector autocorrelation functions for the interior carbons exhibit long-time tail characteristics, which are absent for the carbons close to the chain ends. This long-time tail behavior is found to be the source of the experimental NOE values being less than 3. Correlation times for the torsional autocorrelation function and C–H vector reorientation for the interior carbons correspond closely to the average conformational transition times, indicating the importance of torsional transitions in both the decay of the torsional autocorrelation function and reorientation of the C–H vectors. Experimental T_1 values for PE melts and the interior carbons of C_{44} melts were found to differ by a factor of 2, indicating that the respective rates of conformational transitions are similar. Moreover, simulation results indicate a very strong correlation of conformational transitions with second neighbors and to a lesser extent with fourth neighbors. Consideration of the overall dynamics of self-diffusion, long-time tails in the torsional autocorrelation function and C–H vector reorientation, and correlation in conformational transitions will be presented in a future paper.

Acknowledgment. W.Z. and M.D.E. acknowledge support from the Polymers Program of the National Science Foundation (Grant DMR-9123288). NMR experiments were performed in the Instrument Center of the Department of Chemistry, University of Wisconsin. We thank Professor Alan Jones for discussions on NMR. G.D.S. acknowledges support provided by NASA through Eloret Contract NAS2-14031.

References and Notes

(1) Smith, G. D.; Yoon, D. Y. *J. Chem. Phys.* **1994**, *100*, 649.
(2) In an upcoming paper, we will consider long-time dynamics and correlation of conformational transitions in C_{44} melts.
(3) Glowinkowski, S.; Gisser, D. J.; Ediger, M. D. *Macromolecules* **1990**, *23*, 3520.
(4) Lyerla, J. R., Jr.; McIntyre, H. M.; Torchia, D. A. *Macromolecules* **1974**, *7*, 11.
(5) Dechter, J. J.; Axelson, D. E.; Dekmezian, A.; Glotin, A.; Mandelkern, L. *J. Polym. Sci., Polym. Phys. Ed.* **1982**, *20*, 641.
(6) Flory, P. J. *Statistical Mechanics of Chain Molecules*; Wiley: New York, 1969.
(7) Ovchinnikov, Y. K.; Anitpov, E. M.; Markova, G. S.; Bakeev, N. F. *Makromol. Chem.* **1976**, *177*, 1567.
(8) Viovy, J. L.; Monnerie, L.; Brochon, J. C. *Macromolecules* **1983**, *16*, 1845.
(9) English, A. D.; Dybowski, C. R. *Macromolecules* **1984**, *17*, 446.
(10) Schaefer, J. *Macromolecules* **1972**, *5*, 427.
(11) Gisser, D. J.; Glowinkowski, S.; Ediger, M. D. *Macromolecules* **1991**, *24*, 4270.
(12) Helfand, E.; Wasserman, Z. R.; Weber, T. A. *J. Chem. Phys.* **1979**, *70*, 2016.
(13) Helfand, E.; Wasserman, Z. R.; Weber, T. A. *Macromolecules* **1980**, *13*, 526.
(14) Helfand, E. *J. Chem. Phys.* **1978**, *69*, 1010.